Direct Measurement of the Band Structure of a One-Dimensional Surface Superlattice

B. Kardynał, C. H. W. Barnes, E. H. Linfield, D. A. Ritchie, K. M. Brown, G. A. C. Jones, and M. Pepper
Cavendish Laboratory, Madingley Road, Cambridge, CB3 0HE, United Kingdom
(Received 23 October 1995)

We present a measurement of equilibrium tunneling between a two-dimensional electron gas and a one-dimensional surface superlattice in a double quantum well system. We interpret the tunneling characteristics within the tunneling Hamiltonian formalism and show that the regular series of peaks observed reflects the crystal part of the band structure of the superlattice. In addition, by comparing experiment to theory, we find an approximation to the effective potential of the superlattice. [S0031-9007(96)00223-2]

PACS numbers: 73.40.Gk, 73.20.Dx

Despite the considerable effort which has been put into the study of one-dimensional surface superlattices (1DSSL) [1], no direct measurements of their band structure appear in the literature. However, many of the physical properties of a 1DSSL may be traced back to features in its band structure. For example, conductance measurements show minima due to band gaps [2], and capacitance measurements show a peak when tightly bound states pass through the Fermi energy [3]. The form of the interaction between light and electrons in mesoscopic systems has ruled out optical spectroscopy as a method for determining the band structures of the effective potentials [4]. However, no such problem arises with electron spectroscopy and many measurements of such band structures have been performed by this method [5–11,13]. For example, Hayden *et al.* [9] have used magnetoresonant tunneling spectroscopy to measure the band structure of an atomic surface superlattice. Their measurements showed anisotropy in the higher 2D subbands of a quantum well grown on the GaAs(311)*A* surface.

The advent of double quantum well (DQW) systems has introduced a powerful new tool for performing tunneling spectroscopy measurements [10–12]. In such systems, each two-dimensional electron gas (2DEG) can be independently contacted and the Fermi wave vectors can be independently adjusted using back and front gates [11,14], which allows equilibrium tunneling spectroscopy measurements. In addition, and crucial to this work, the front gate can be patterned so that the potential in the upper 2DEG may be modulated while leaving the lower 2DEG virtually free from modulation [6,12,15].

In this Letter, we report the first equilibrium electron tunneling spectroscopy measurement of a 1DSSL. The samples are modulation doped DQW structures, grown using molecular-beam epitaxy. Each sample contains two 18 nm wide GaAs wells, separated by an undoped 12.5 nm $Al_{0.33}Ga_{0.67}As$ barrier. The upper well is 70 nm below the surface. Si-doped layers placed above and below the DQW populate the lowest subband of each well with 2DEGs of nominal density 3.0×10^{15} and $1.8 \times 10^{15}\ m^{-2}$ in the upper and lower wells, respectively, with the corresponding low temperature mobilities of 80 and $20\ m^2\ V^{-1}\ s^{-1}$. The mesa and the Ohmic contacts to the 2DEGs and the back gates were fabricated using standard processes. *In situ* focused ion beam implantation below the contacts to the 2DEGs was used to prevent leakage between the 2DEGs and the back gates [16]. The 2DEG Ohmic contacts connect both 2DEGs together and a selective depletion scheme was used to allow contact to each 2DEG independently [14,17].

The inset to Fig. 1 shows a schematic diagram of the device. The back gate is continuous and covers the complete tunneling area. The front gate is patterned by electron beam lithography into a grating of fifty one gates, connected by a single gate. It separates the active tunneling area into three different regions: (A1) the 1DSSL, (A2) a region with no gate, and (A3) a region with a continuous gate.

For the present work we concentrate on a 1DSSL with period 570 nm and lithographic gate width 230 nm (and areas A1, A2, and A3 of 880, 780, and 290 μm^2, respectively). We briefly mention the results of the

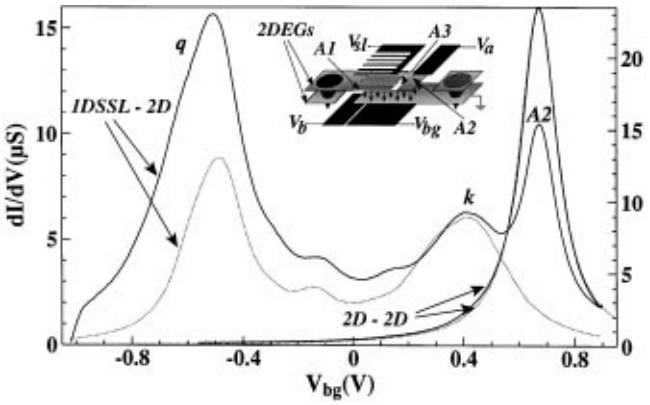

FIG. 1. Solid lines: experimental TDC, for 2D-2D ($V_{sl} = 0.03$ V) and 1DSSL-2D ($V_{sl} = -0.25$ V) tunneling. Dotted lines: calculated TDC. TDC for 1DSSL-2D tunneling was calculated using the potential form shown in Fig. 4. Inset: Diagram of the device. V_a and V_b define independent contact to each layer. V_{sl} and V_{bg} control the tunneling area of the device.

 0031-9007/96/76(20)/3802(4)$10.00

measurements of devices with periods 350 and 680 nm and gate widths 180 and 200 nm, respectively. These will be fully discussed in a longer article. By applying a voltage V_{sl} to the superlattice gate, the 1DSSL potential modulation in the top well could be varied from zero to the Fermi energy. The tunneling differential conductance (TDC) between 2DEGs was measured at a temperature of 300 mK in a two terminal configuration with an excitation voltage of 100 μV at 79 Hz. The observed structure did not change when smaller excitation voltages were used. The TDC was measured as a function of back-gate voltage V_{bg}, with zero dc bias applied between the wells, i.e., effectively as a function of the Fermi energy of electrons in the lower well. This method eliminated the possibility that the structure observed in the TDC originates from the in-plane conductance in the 1DSSL.

2D-2D resonant tunneling is shown for our device in Fig. 1. The TDC has a very sharp maximum at $V_{bg} = +0.67$ V, where the carrier concentrations in both 2DEGs are matched and the conditions of total energy and in-plane momentum conservation required for resonant tunneling are fulfilled. It was found to be necessary to apply $V_{sl} = +0.03$ V to the superlattice gate in order to compensate the strain potential introduced in the upper 2DEG by this gate [18]. The 2D-2D tunneling characteristic suggests that the potential modulation in the lower 2DEG is negligible, or considerably smaller than the line width of the peaks.

When a negative voltage is applied to the superlattice gate, the single 2D-2D tunneling peak splits into three large 2D-2D tunneling peaks and a regular set of smaller peaks. An example is shown in Fig. 1 for $V_{sl} = -0.25$ V, in which the three large peaks have been labeled k, q, and A_2. The k peak derives from tunneling into the 2DEG in the ungated region of A1. The q peak derives from the gated region of A1 and the region A3, and the A2 peak derives from the region A2. The peaks occur at back-gate voltages where the carrier concentrations in the lower 2DEG and in relevant parts of the upper 2DEG are matched. They have amplitudes proportional to the area of these parts of the upper 2DEG.

The smaller peaks reflect the crystal part of the 1DSSL band structure. Their positions correspond approximately to back-gate voltages where, at the Fermi energy, k_y in the 2DEG is equal to k_y in the 1DSSL to within reciprocal lattice vector $G_n = 2n\pi/(a + b)$. n is an integer, $a + b$ is the 1DSSL grating period, and the y direction is perpendicular to the 1DSSL gates. As a consequence, when the period of the grating was changed from 670 to 350 nm the spacing between the peaks increased and hence their number decreased as shown in Fig. 2. Each trace has had the gross background removed, using a high pass filter, to reveal only the 1DSSL band structure. Figure 3(a) shows a gray scale plot of a series of experimental TDC traces taken with the 1DSSL period of 570 nm and potential amplitude varying between zero, $V_{sl} = +0.03$ V, and the Fermi energy, $V_{sl} = -0.35$ V. Each trace was filtered in the same way as for Fig. 2—white corresponds to a peak.

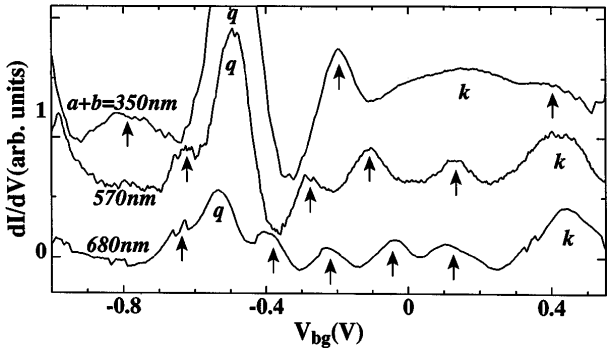

FIG. 2. TCD for $V_{sl} = -0.25$ V for three different period gratings. Arrows mark the peaks, which are due to the crystal part of the 1DSSL band structure.

The exact positions of the smaller peaks requires analysis of the electron states in the 1DSSL and the 2DEG and their contribution to the tunneling. The low temperature TDC for tunneling between 2DEG and 1DSSL within

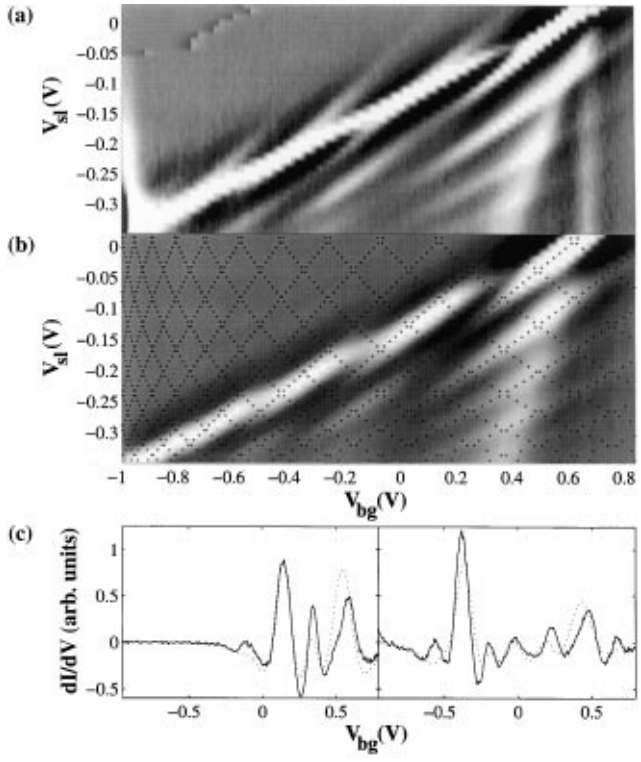

FIG. 3. (a) TDC characteristics taken for $V_{sl} = [+0.03\text{ V}, -0.35\text{ V}]$. The gross background has been removed to reveal the 1DSSL band structure—white peaks. (b) Theory corresponding to (a) using the potential shape shown in Fig. 4 with an overlay dot pattern showing the corresponding crystal band structure. (c) Comparison of filtered experimental (full line) and theoretical (dotted line) TDC for $V_{sl} = -0.13$ V (left) and -0.22 V (right).

transfer Hamiltonian formalism [20,21] is given accurately by

$$dI/dV \propto t^2 \sum_{k_x,k_y} B_1(k_x,k_y;\mu)A_2(k_x,k_y;\mu). \quad (1)$$

The augmented spectral function of the 1DSSL B_1 is defined as

$$B_1(k_x,k_y;\mu) = \sum_{\nu} |\tilde{\varphi}_{k_y,\nu}(-k_y)|^2 A_1(k_x,k_y,\nu;\mu). \quad (2)$$

In the quasiparticle approximation the spectral functions of the 1DSSL and 2DEG, $A_{(1,2)}$, are Lorentzian

$$A_{(1,2)}(s_{(1,2)};\mu) = \Gamma/2\pi[(\Gamma/2)^2 + (\mu - \xi^{(1,2)}_{s_{(1,2)}})^2], \quad (3)$$

$s_1 = (k_x, k_y, \nu)$, $s_2 = (k_x, k_y)$ are the quantum numbers for the 2DEG and 1DSSL, respectively, $\hbar/\Gamma$ is the quasiparticle lifetime, t^2 is the z-direction transmission coefficient (assumed energy and position independent), and μ is the electrochemical potential. $\xi^{(2)}_{s_2} = (\hbar^2/2m^*)(k_x^2 + k_y^2) + V_2$ is the energy dispersion relation of the 2DEG. We used the dispersion relation of the 1DSSL in the form $\xi^{(1)}_{s_1} = \hbar^2 k_x^2/2m^* + E_{k_y,\nu} + V_1$, where $E_{k_y,\nu}$ is the crystal part of the 1DSSL band structure and ν is the band index. $V_{(1,2)}$ are the energy levels of the 2D subbands in the upper and lower wells, respectively. We write the wave function perpendicular to the 1DSSL in the Bloch form: $\phi_{k_y,\nu}(y) = \sum_n e^{ik_y n(a+b)} \varphi_{k_y,\nu}(y - n(a+b))$, where $\varphi_{k_y,\nu}(y)$ is a solution of the Schrödinger equation for the 1DSSL potential for $0 \le y < a + b$ and is zero elsewhere. $\tilde{\varphi}_{k_y,\nu}(k)$ in Eq. (2) is the Fourier transform of $\varphi_{k_y,\nu}(y)$.

In the limiting case of zero potential amplitude in the 1DSSL Eq. (1) represents tunneling between two 2DEGs and takes the form of an overlap between the two spectral functions of the 2DEGs at the Fermi energy (which are the disorder broadened Fermi circles). The best fit, using Eq. (1) for zero potential modulation, to the 2D-2D tunneling peak is shown as a dotted line in the inset of Fig. 1 and has $\Gamma \sim 0.5$ meV. Similar values of Γ have been seen in other experiments on 2D-2D tunneling [14,19] confirming the assumption of the negligible potential modulation in the lower 2DEG.

When the 1DSSL potential is defined parallel to $y = 0$ a set of Brillouin zone boundaries appear parallel to $k_y = 0$. This has the effect that, in the extended zone scheme, a cut through a spectral function of the 1DSSL at the Fermi energy appears as a set of circles displaced by reciprocal lattice vectors G_n. In addition, if the 1DSSL wells are sufficiently deep, a set of tightly bound Bloch states form. Having no dispersion in k_y, they appear as a set of lines running parallel to $k_x = 0$. Figure 5(a) shows such a cut for the 1DSSL potential shown in Fig. 4 at the experimental Fermi energy 11.0 meV. It was calculated using Eq. (3) and dispersion relation for the 1DSSL given above.

It is the augmented spectral function B_1 however which, in accordance with Eq. (1), is the key to understanding

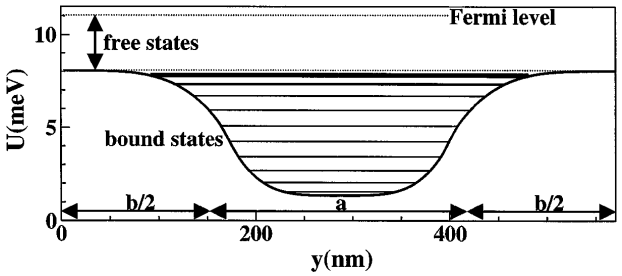

FIG. 4. 1DSSL potential, which gave the best agreement between experiment and theory, with corresponding eigen spectrum.

equilibrium tunneling spectroscopy of the 1DSSL. The TDC is the overlap of B_1 (and not A_1) with the disorder broadened Fermi circle of the 2DEG (A_2). B_1 makes a rather striking pattern and an example is shown in Fig. 5(b) again using the potential form shown in Fig. 4. For the bound states, $\nu = 1, 2, \ldots, 10$, the wave functions $\varphi_{k_y,\nu}$ are only weakly dependent on k_y so that $\tilde{\varphi}_{k_y,\nu}(-k_y)$ is approximately the Fourier transform of these wave functions. The vertical lines in Fig. 5(a) are then replaced in Fig. 5(b) by the modulus squared of the Fourier transforms of the bound state wave functions. This has been noted for 1D-2D and 1D-1D nonequilibrium tunneling [8,22,23]. The difference between Figs. 5(a) and 5(b) for the free states, $\nu > 10$, is most easily illustrated using the Kronig-Penney wave functions. They have the form $\phi_{k_y,\nu}(y) = A\exp(iky) + B\exp(-iky)$ in the ungated regions of A1 and $\phi_{k_y,\nu}(y) = C\exp(iqy) + D\exp(-iqy)$ in the gated regions. For such wave functions $|\tilde{\phi}_{k_y,\nu}(-k_y)|^2$ clearly contains peaks at $k_y = \pm k$ and $k_y = \pm q$. In going from the abrupt Kronig-Penney model to a smoother potential these peaks are still present but are broadened. These peaks give B_1 in Fig. 5(b) the rough appearance of two dark concentric circles (high tunneling probability). Experimentally this gives rise to the bright k and q peaks of the TDC in Fig. 3(a).

The experimental positions of the k and q peaks in TDC characteristics determine the minimum and maximum of the effective 1DSSL potential since they tell us the

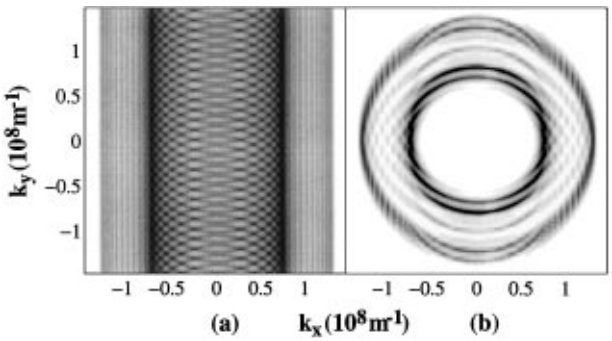

FIG. 5. (a) A cut through the spectral function A_1 of the 1DSSL potential shown in Fig. 4 at 11.0 meV. (b) Same as (a) for the augmented spectral function B_1.

electron concentration in the ungated and gated regions of the 1DSSL, respectively. The positions of the smaller (band structure) peaks are determined by the shape of the potential. By evaluating the TDC using Eq. (1), for the potential shown in Fig. 4 we find the characteristic shown as a dotted line in Fig. 1. A direct comparison between the experimental and theoretical traces in Fig. 1 is not possible since the q and A2 peaks of the experimental trace are greatly enhanced by tunneling from the areas A2 and A3 of the device. However, the positions of the smaller peaks are not affected by this extra tunneling and for these we can directly compare experiment and theory. We have calculated a theoretical trace corresponding to each experimental trace in Fig. 3(a). The resulting gray scale is shown in Fig. 3(b) and may be compared directly with Fig. 3(a).

The potential used for each trace has the shape given in Fig. 4. The amplitude and mean were scaled to give the k and q peaks in the correct experimental positions. This potential is the best fit obtained from a series of calculations for different potential shapes, varied continuously from triangular to square, and with variable aspect ratio a/b (defined in Fig. 4), but fixed $a + b = 570$ nm (superlattice gate period). In principle a more accurate estimate of the shape of effective potential, including its dependence on V_{s1}, could have been determined by fitting each TDC characteristic individually had a direct comparison between experimental and theoretical TDC traces been possible.

An example of a comparison between experimental and theoretical TDC (both with gross background removed) for $V_{s1} = -0.13$ and -0.22 V, is shown in Fig. 3(c). It demonstrates that the distance between peaks is consistent with the 1DSSL period. This was the case in all devices measured. Figure 3(b) shows a pattern of dots which correspond to the points where the condition $k_y^{2\mathrm{DEG}} = k_y^{1\mathrm{DEG}} + G_n$ is satisfied for the superlattice gate voltages used in the experiment. This pattern, which represents the crystal part of the band structure of the 1DSSL, follows the centers of the white bands in most regions of the gray scale accurately. Therefore despite the complexity of B_1 we can justify our claim that the measurement gives directly the crystal part of a 1DSSL band structure.

The dot pattern in Fig. 3(b) has lines with both positive gradients (normal tunneling processes) which are seen experimentally and negative gradients (umklapp tunneling processes) which are not. Within our formalism the main reasons for this is clear from comparison of Figs. 5(a) and 5(b). B_1 itself contains little of the band structure which refers to umklapp processes since 1DSSL states with positive momentum have little contribution from plane wave states with negative momentum and *vice versa*.

In conclusion, we have demonstrated that equilibrium electron tunneling spectroscopy in a double quantum well structure is an accurate and direct probe of the band structure of a 1DSSL. We are able to measure clearly the normal tunneling processes between wells but find that the umklapp tunneling processes are washed out. We find that one should expect small deviations of the experimental peak positions from the pure crystal band structure since the peaks correspond to the maximum of the overlap of the disorder broadened Fermi circle of the 2DEG and the augmented spectral function of the 1DSSL. By fitting the experimental data using the tunneling Hamiltonian formalism we are able to construct an approximation to the 1DSSL effective potential.

We would like to thank C. J. B. Ford, A. R. Hamilton, J. T. Nicholls, and D. Khmelnitskii for helpful discussions. B. K. acknowledges support from Trinity College. D. A. R. acknowledges support from Toshiba Cambridge Research Center. This work was funded by the EPSRC.

[1] C. W. J. Beenakkerand H. van Houten, in *Solid State Physics*, edited by H. Ehrenreich and D. Turnbull (Academic Press, San Diego, 1991), Vol. 44.
[2] K. Ismail *et al.*, Appl. Phys. Lett. **52**, 1071 (1988).
[3] T. P. Smith *et al.*, Phys. Rev. Lett. **59**, 2802 (1987).
[4] W. Hansen, in *Proceedings of the 39th Scottish Universities Summer School in Physics, St. Andrews, Scotland, 1991* (Scottish Universities Summer School in Physics & Adam Hilger, Bristol, Philadelphia 1991).
[5] U. Genner *et al.*, Phys. Rev. Lett. **67**, 2828 (1991).
[6] W. Demmerle *et al.*, Phys. Rev. B **44**, 3090 (1991); Semicond. Sci. Technol. **6**, 839 (1991).
[7] S. Y. Lin *et al.*, Appl. Phys. Lett. **60**, 601 (1992); Appl. Phys. Lett. **60**, 2812 (1992).
[8] J. Wang *et al.*, Phys. Rev. Lett. **73**, 1146 (1994).
[9] R. K. Hayden *et al.*, Semicond. Sci. Technol. **9**, 298 (1994).
[10] J. P. Eisenstein *et al.*, Phys. Rev. B **44**, 6511 (1991).
[11] K. M. Brown *et al.*, Appl. Phys. Lett. **64**, 1827 (1994).
[12] J. Smoliner *et al.*, Semicond. Sci. Technol. **9**, 1925 (1994).
[13] A. Kurobe *et al.*, Phys. Rev. B **50**, 4889 (1994).
[14] J. P. Eisenstein *et al.*, Appl. Phys. Lett. **57**, 2324 (1991); Appl. Phys. Lett. **58**, 1499 (1991).
[15] B. Kardynal *et al.*, Appl. Phys. Lett. **68**, 826 (1996).
[16] E. H. Linfield *et al.*, Semicond. Sci. Technol. **9**, 415 (1993).
[17] K. M. Brown *et al.*, J. Vac. Sci. Technol. B **12**, 1293 (1994).
[18] J. H. Davies and I. A. Larkin, Phys. Rev. B **49**, 4800 (1994).
[19] K. M. Brown *et al.*, in *Proceedings of the ICPS Conference, Vancouver* (World Scientific, Singapore, 1994), p. 1035.
[20] G. D. Mahan, *Many-Particle Physics* (Plenum Press, New York, 1993), 2nd ed.
[21] L. Zheng and A. H. MacDonald, Phys. Rev. B **47**, 10 619 (1993).
[22] W. Demmerle *et al.*, Phys. Rev. B **47**, 13 574 (1993).
[23] N. Mori *et al.*, Phys. Rev. B **51**, 1735 (1995).